JGR Space Physics

RESEARCH ARTICLE
10.1029/2023JA031411

# GPS Loss of Lock Events and Their Dependence on the Interplanetary Magnetic Field Orientation

**G. Lovati[1,2], P. De Michelis[2], G. Consolini[3], M. Pezzopane[2], A. Pignalberi[2], and F. Berrilli[4]**

[1]Dipartimento di Fisica, Universitá di Roma Sapienza, Rome, Italy, [2]Istituto Nazionale di Geofisica e Vulcanologia, Rome, Italy, [3]INAF-Istituto di Astrofisica e Planetologia Spaziali, Rome, Italy, [4]Dipartimento di Fisica, Universitá di Roma Tor Vergata, Rome, Italy

**Key Points:**

- The number of Global Positioning System (GPS) loss of lock (LoL) events is affected by the interplanetary magnetic field (IMF) orientation
- GPS LoLs are most common at the cusp, the area of separation between two convection cells, and the nightside of the auroral oval
- The duration of GPS LoL events does not appear to be affected by the strength of the IMF

**Correspondence to:**
P. De Michelis,
paola.demichelis@ingv.it

**Citation:**
Lovati, G., De Michelis, P., Consolini, G., Pezzopane, M., Pignalberi, A., & Berrilli, F. (2023). GPS loss of lock events and their dependence on the interplanetary magnetic field orientation. *Journal of Geophysical Research: Space Physics*, *128*, e2023JA031411. https://doi.org/10.1029/2023JA031411

Received 16 FEB 2023
Accepted 29 JUN 2023

**Author Contributions:**
**Conceptualization:** G. Lovati, P. De Michelis, G. Consolini
**Data curation:** M. Pezzopane, A. Pignalberi
**Formal analysis:** G. Lovati, G. Consolini
**Investigation:** P. De Michelis
**Methodology:** G. Lovati
**Supervision:** P. De Michelis, F. Berrilli
**Writing – original draft:** G. Lovati, P. De Michelis
**Writing – review & editing:** G. Lovati, P. De Michelis, G. Consolini, M. Pezzopane, A. Pignalberi



**Abstract** The study investigates the influence of interplanetary magnetic field (IMF) orientation on loss of lock (LoL) events in Global Positioning System signals. We analyzed LoLs recorded on two Swarm satellites between July 2014 and December 2021, examining how the signs of the IMF $B_x$, $B_y$, and $B_z$ components affect the distribution of events at high latitudes. Our results reveal an asymmetric distribution of LoL events over 75° magnetic latitude. In the Northern hemisphere, more events occur in the post-noon sector with negative IMF $B_y$, and in the pre-noon sector with positive IMF $B_y$. Conversely, in the Southern hemisphere, pre-noon events increase with negative IMF $B_y$, while post-noon events increase with positive IMF $B_y$. At lower latitudes (50°–75°), IMF $B_y$ does not significantly affect the event distribution, which mainly concentrates in the night sector for both hemispheres. Additionally, we found a connection between IMF $B_y$ and $B_x$, primarily due to the IMF spiral structure. Finally, we discuss our findings in the context of the SuperDARN data-driven model of ionospheric convection patterns, which shows that LoL events frequently cluster in the cusp region, as well as the area where the two convection cells separate.

## 1. Introduction

Global Navigation Satellite Systems (GNSS) play a crucial role in modern society thanks to its growing dependence on precise positioning, navigation, timing, and synchronization techniques. The American Global Positioning System (GPS) and its Russian counterpart GLONASS are currently in use in this context, along with the Chinese BeiDou, the European Galileo, and other regional systems such as the Indian IRNSS or the Japanese QZSS. GNSS signals operate in the L-band frequency domain, which falls within the radio spectrum and covers frequencies between 1 and 2 GHz. Moreover, to account for ionospheric delays in their measurements, these systems employ at least two different frequencies (Teunissen & Montenbruck, 2017). When traveling from a GNSS satellite to a receiver either onboard a low Earth orbit satellite or on the ground, signals pass through the ionosphere and interact with its charged particles. The presence of irregularities in plasma density is one of the ionospheric phenomena that significantly lowers the performance of GNSS. In fact, variations in ionospheric electron density can affect both the phase and amplitude of electromagnetic waves propagating through it, and thus GNSS signals. In the worst-case scenario, signals might be disrupted, causing the receiver to lose track of a transmitting satellite. This type of event is known as loss of lock (LoL), which can result in a decrease in GNSS positioning accuracy and the inability to obtain total electron content (TEC) measurements. This last mentioned quantity represents an integral measurement of the TEC along the signal path from the satellite to the receiver.

The harmful effects of GPS LoL events have been extensively studied in recent years to determine the most affected regions and the circumstances that trigger their onset. They have been discovered to happen more frequently under specific conditions, such as increased solar activity (Liu et al., 2017; Pezzopane et al., 2021) and geomagnetic storms (Jin & Oksavik, 2018; Zhang et al., 2020). In terms of the most affected locations, GPS LoLs seem to occur in three distinct magnetic latitude (MLat) bands: one near the magnetic equator and the other two at high latitudes, above 50° for the Northern hemisphere and below −50° for the Southern one. While the majority of GPS LoL events appear to be linked to equatorial plasma bubbles at low latitudes (Buchert et al., 2015; De Michelis et al., 2022), the situation is more complex at high latitudes and no clear explanation has been found yet.

At high latitudes, the interplanetary magnetic field (IMF), which is carried to the Earth system by the solar wind, is closely related to the macroscopic motion of the ionospheric plasma. The ionospheric convection pattern in the plane perpendicular to the magnetic field lines, which corresponds to the horizontal motion of plasma, has

been found to be highly dependent on the orientation and magnitude of the IMF. According to Cowley (1982), the IMF plays a dominant role in magnetic reconnection on the dayside magnetopause. When the magnetic field, which is frozen in the solar wind plasma, meets the Earth's magnetic field in a favorable orientation, energy, and momentum can be transferred from the solar wind to the magnetosphere and plasma motion can occur in the coupled magnetosphere-ionosphere system. In the ionosphere, the resulting convection motion can be seen as an antisunward flow over the polar cap, from the noon sector to the midnight sector, and a sunward return flow at lower latitudes, on both the dawn and dusk flanks of the auroral oval zone. That produces a two-cell ionospheric flow pattern (Tanaka, 2007), which is more or less fixed with respect to the Sun-Earth line. The most favorable orientation for this phenomenon is the southward IMF. When the IMF has a northward component ($B_z > 0$), a noticeable departure from the previously described convection patterns is observed. Although reconnection can still occur for positive $B_z$ values, it will take place poleward with respect to the magnetic cusp. This can lead to a flow toward the Sun over the polar cap, resulting in smaller and reversed convection cells (Fear, 2021). Furthermore, the region of significant plasma motion is considerably restricted to higher latitudes compared to the southward IMF. In this case, four convection cells are typically observed in the dayside hemisphere, with their size and orientation predominantly influenced by the magnitude and sign of IMF $B_y$ component (Cowley et al., 1991). The high-latitude convection pattern can also be influenced by the IMF $B_x$ component. When using the "dipole plus uniform field" model, IMF $B_y$ component produces an asymmetry with respect to the noon-midnight meridian, while IMF $B_x$ component creates an asymmetry with respect to the dawn-dusk meridian (Cowley et al., 1991). However, in the literature, the effect of the IMF $B_x$ component is often overlooked, and most of the empirical functions proposed to describe the solar wind-magnetosphere-ionosphere coupling only consider the $B_z$ and $B_y$ components (Peng et al., 2010). The spiral structure of the IMF leads to a strong negative correlation between $B_x$ and $B_y$ components. As a result, a positive sign of one component is usually associated with a negative sign of the other one (Cowley et al., 1991; Karpachev et al., 1995). This means that the effect of the IMF $B_x$ component may already be accounted for when considering the $B_y$ component alone. Therefore, some empirical functions used to describe the solar wind-magnetosphere-ionosphere coupling may implicitly include the influence of the $B_x$ component, even if it is not explicitly included (Peng et al., 2010).

It has been found that the spatial distributions of plasma density irregularities depend on the IMF orientation (Lockwood et al., 2000; Moen et al., 2008; Tsunoda, 1988). For instance, Jin et al. (2019) demonstrated how the IMF's $B_y$ component affects the distribution of the plasma density irregularities in the cusp and polar cap regions, resulting in an interhemispheric asymmetry in the spatial distribution of these irregularities. This finding agrees with the high-latitude ionospheric convection pattern. Furthermore, it has been shown that when the IMF $B_y$ component is negative, there is a notable difference between the Northern and Southern hemispheres in the distribution of ionospheric irregularities near the cusp and in the polar cap region: in the Northern hemisphere, the irregularities are more numerous in the postnoon sector, while in the Southern hemisphere they are more numerous in the prenoon sector. On the other hand, Jin et al. (2020) studied the effect of the IMF $B_z$ component on the ionospheric plasma irregularities. They revealed that negative values of IMF $B_z$ component cause a higher concentration of irregularities to occur at lower magnetic latitudes, compared to positive $B_z$ values. Evidence of IMF dependence has also been discovered for polar cap patches, which are one of the most important phenomena related to high-latitude ionospheric irregularities (Spicher et al., 2017).

The occurrence of GPS LoL events is commonly linked with ionospheric irregularities, which suggests that the configuration of the IMF may also influence the development and spatio-temporal distribution of these events. In this study, we aim to investigate whether specific IMF configurations can favor the occurrence of LoLs and affect their spatial distribution. To explore this relationship, we analyzed GPS LoL events recorded by the European Space Agency's (ESA) Swarm mission between mid-July 2014 and the end of 2021. We examined the distributions of these events at high latitudes in magnetic latitude/magnetic local time (MLT) coordinates and assessed their statistical dependence on the orientation of the IMF. The results were then discussed in detail, taking into consideration the reconstructed ionospheric convection patterns obtained via SuperDARN model.

## 2. Data and Processing Approach

We used data from the Swarm mission, which is an ongoing ESA constellation mission for Earth Observation (Friis-Christensen et al., 2008). It consists of three identical satellites known as Swarm A, B, and C, all of which are equipped with the same set of instruments that measure electric and magnetic fields, as well as plasma density

and temperature. They were launched on 22 November 2013, into two distinct near-polar orbits: A and C are in a low-Earth orbit at an initial altitude of about 480 km, while B is in a higher low-Earth orbit at an initial altitude of about 530 km. The three satellites are also equipped with Precise Orbit Determination (POD) antennas, that are GPS receivers, necessary to precisely locate the electric, magnetic, and plasma measurements (van den IJssel et al., 2015). Swarm GPS tracking data are also required to calculate the slant Total Electron Content (sTEC), which is the integrated electron density along the line of sight from one Swarm satellite to each GPS satellite in its field of view.

For the current analysis, we use the sTEC time-series, collected onboard Swarm A and B, to identify the GPS LoL events. It is important to note that sTEC measurements are only possible when both values of the ambiguity-corrected carrier phase observations from the POD antenna are available. If one or both values are unavailable, two possibilities exist: either the GPS satellite has left the POD antenna's field of view, or a LoL event is occurring. To rule out the first phenomenon, we classified as LoL events only interruptions in the sTEC time series that lasted less than 1,200 s (Pezzopane et al., 2021). Additionally, because it has been found that LoL events lasting 1 s may not actually be real, we excluded them from our data set (Pezzopane et al., 2021). The sTEC time-series are Level 2 data that can be downloaded from the ESA dissemination server (ftp://swarm-diss.eo.esa.int), where they are available at a time resolution of 0.1 Hz until 14 July 2014, when the sampling frequency was increased to 1 Hz. We limited our analysis to the period between 15 July 2014 and 31 December 2021. Additionally, we focused on the mid- and high-latitude regions in both hemispheres.

We used IMF $B_x$, $B_y$, and $B_z$ components downloaded from the NASA OMNI Web Data Explorer website (https://omniweb.gsfc.nasa.gov/form/dx1.html) to see if the IMF has any influence on the occurrence and geographical distribution of GPS LoL events. The ACE and Wind spacecrafts, which are both near L1 Lagrange point, provided the IMF measurements at 1 min cadence. These data are successively time-shifted to the Earth's bow shock's nose. The left column of Figure 1 illustrates the distributions of the three IMF components during the considered time period. The resulting joint Probability Density Function (PDF) for IMF $B_y$ and $B_z$ components is presented in the first row on the left. The distribution displays two symmetrical peaks with respect to both the $B_y = 0$ and $B_z = 0$ axes. Both are centered around the value of IMF $B_z = 0$, while IMF $B_y \simeq \pm 2$ nT. The joint PDF for IMF $B_x$ and $B_y$ components can be found in the second row of on the left of Figure 1. The distribution displays two peaks that are roughly located on the bisector $B_y = -B_x$. This behavior can be explained by the spiral structure of the IMF, where a positive sign of the IMF $B_y$ component is often accompanied by a negative sign of the IMF $B_x$ component, and vice versa (Karpachev et al., 1995).

To assign appropriate values of the IMF components that could have triggered favorable ionospheric conditions for each GPS LoL event, it is necessary to consider the time delay required for the IMF to produce variations in the magnetospheric-ionospheric convection system. It is not easy to evaluate this delay since it depends on various factors, such as the local time (Murr & Hughes, 2001), the solar wind velocity (Yu & Ridley, 2009), or the type of IMF turning (Dods et al., 2017; Ruohoniemi & Greenwald, 1996). The high-latitude ionospheric convection patterns can be considered as a combination of two time-varying patterns: one resulting from the coupling of the solar wind and magnetosphere at the dayside magnetopause and the other from the release of energy from the geomagnetic tail. The flows caused by the dayside coupling are more prominent on the dayside and typically dominate there. These flows are associated with an expanding polar cap region and exhibit excitation and decay within approximately 10 min after the IMF changes direction to the South and North, respectively (Dods et al., 2017; Ruohoniemi & Greenwald, 1996). The flows resulting from the energy release in the tail, primarily during substorms, are most intense on the nightside, and are associated with a contracting polar cap boundary. These flows are triggered on a timescale of approximately 1 hr after the IMF turns South (Lockwood et al., 1990). Therefore, we approximated the time delay by selecting a value midway between the delay that characterizes MLT around noon (few minutes, Dods et al., 2017; Ruohoniemi et al., 1993) and that of the nightside (∼1 hr, Lockwood et al., 1990). We decided to assign to each LoL event an average IMF value based on the values obtained between 20 and 40 min before the event. This choice appears to be a reasonable timescale for the IMF to induce global effects in the high-latitude ionosphere, and it has previously been used for statistical studies (Coley & Heelis, 1998; Consolini et al., 2021; De Michelis et al., 2017; Jin et al., 2020; Moen et al., 2015).

We only considered the first 5 s of each of the identified LoL events, which ranged in length from 2 to 1,200 s. This decision was forced by the need to be able to accurately identify the IMF orientations that might have led to the occurrence of LoL events in the ionosphere. The joint PDF of the $B_y$ and $B_z$ components, conditioned on the

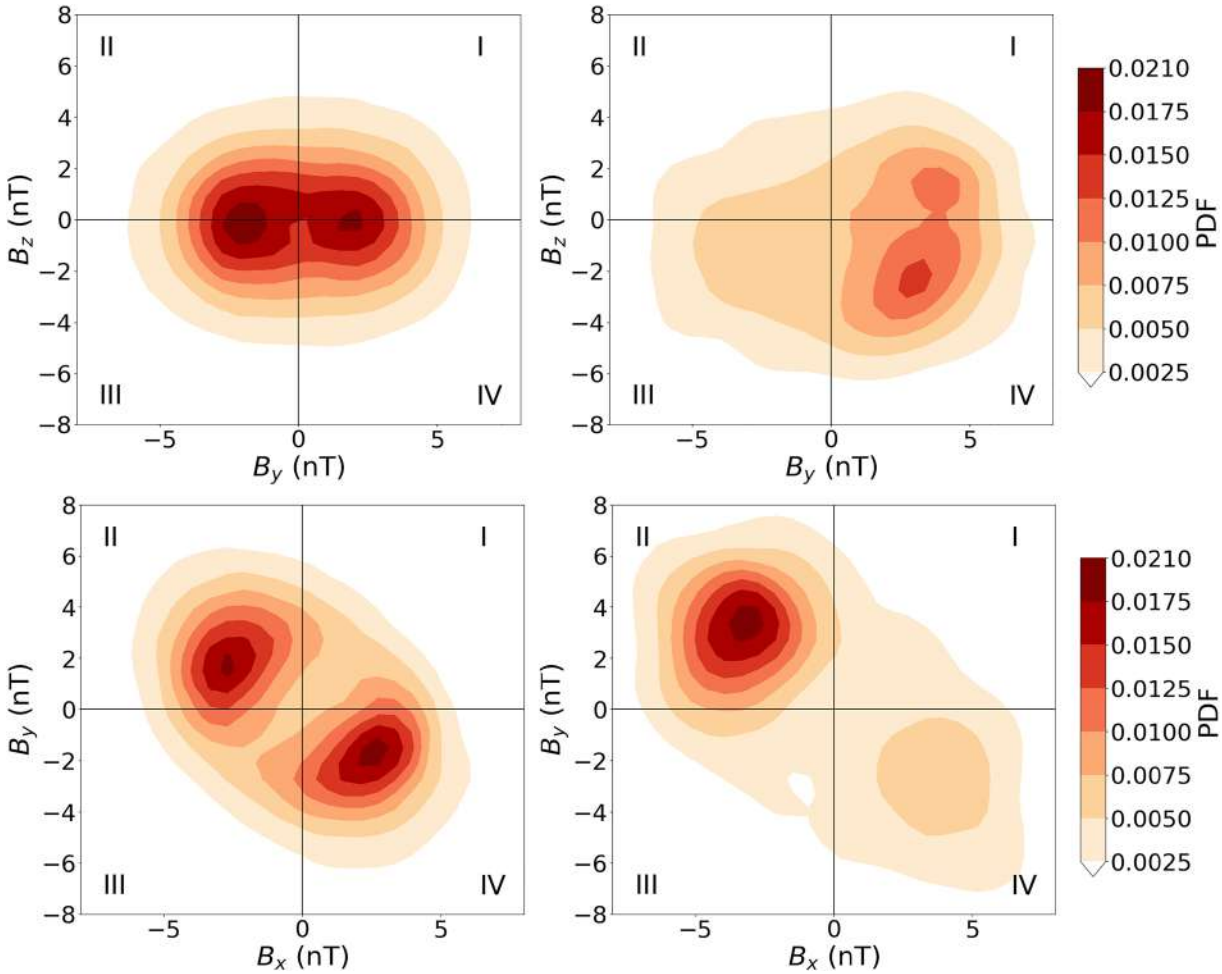


**Figure 1.** In the first row: on the left there is the joint Probability Density Function (PDF) of $B_y$ and $B_z$ obtained from all OMNI data recorded from 15 July 2014 to 31 December 2021, and on the right there is the joint PDF of $B_y$ and $B_z$ conditioned on the occurrence of loss of lock (LoL) events. In the second row: on the left is the joint PDF of $B_x$ and $B_y$ obtained from all OMNI data recorded from 15 July 2014 to 31 December 2021, and on the right is the joint PDF of $B_x$ and $B_y$ conditioned on the occurrence of LoL events.

first 5 s of each GPS LoL event, is shown in the first row of the right column of Figure 1. The joint PDF in the first row of the right column of Figure 1 shows a dominant peak located at $B_y > 0$ and $B_z < 0$, indicating that LoL events are more likely to occur during periods characterized by a specific IMF orientation. A similar trend is observed in the second row of the same column, where the joint PDF of $B_x$ and $B_y$ values, relative to the first 5 seconds of GPS LoL events, exhibits a single main peak for $B_y > 0$ and $B_x < 0$. These results demonstrate that the IMF patterns associated with GPS LoL events differ significantly from those of corresponding to the overall distribution.

## 3. Analysis and Results

Our analysis began by mapping the LoL events recorded by the Swarm satellites during the selected time interval as a function of four different IMF orientations in the geocentric solar magnetospheric (GSM) yz-plane, which define four different sectors. Our goal was to investigate whether LoL event occurrences are influenced by IMF orientation, and to determine whether there exist any spatial pathways privileged for LoL occurrences, as a function of IMF orientation. Figure 2 depicts a polar view of these events in the Northern hemisphere. LoL event maps were generated by arranging data in quasi-dipole (QD) magnetic latitude (MLat) and MLT. When examining phenomena related to horizontally stratified ionospheric currents, the QD coordinate system is preferred over other reference frames, according to Richmond (1995), and is therefore utilized in our analysis. Furthermore,

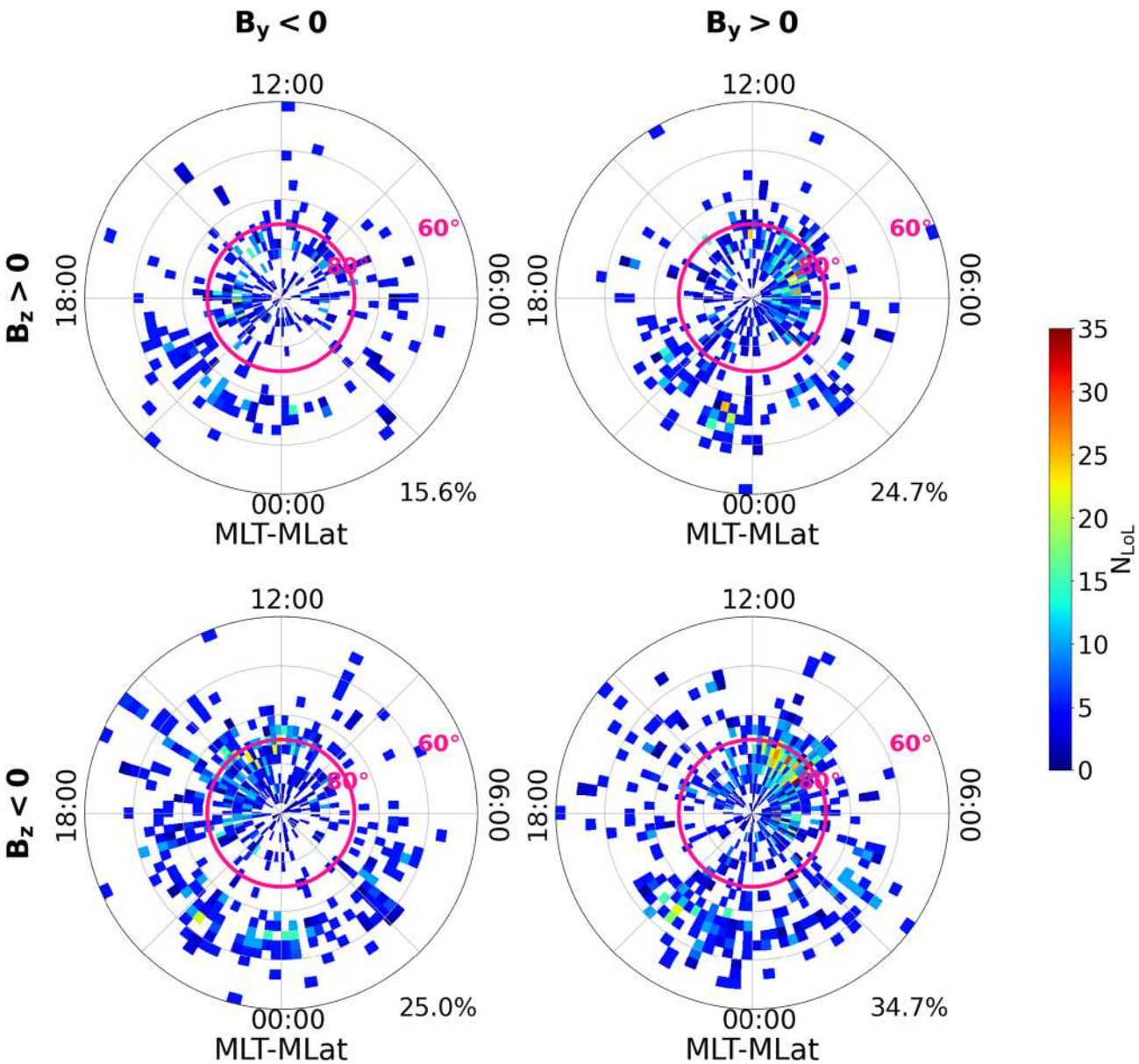


**Figure 2.** Polar view of loss of lock events spatial distribution for the Northern hemisphere in a quasi-dipole magnetic latitude (MLat ≥ 50°N) and magnetic local time reference frame, for four different interplanetary magnetic field (IMF) sectors in the geocentric solar magnetospheric yz-plane. Maps have been drawn using data recorded onboard Swarm A and Swarm B from 15 April 2014 to 31 December 2021. MLat = 75°N can be distinguished by the magenta colored curve. Percentage at bottom right of each plot indicates the fraction of events characterized by that particular IMF configuration, with respect to the total number of events.

instead of QD magnetic longitude, MLT is used to display data relative to the position of the Sun. When the number of LoL events for each IMF sector identified in the GSM yz-plane are compared, it is possible to see that the most populated sector has $B_y > 0$ and $B_z < 0$ (34.7%), while the sector with the most unfavorable conditions has $B_y < 0$ and $B_z > 0$ (15.6%). The remaining two are nearly evenly populated (~25%). The magnetic cusp, which is located around the noon meridian at magnetic latitudes ranging from approximately 70°–85° depending on the level of geomagnetic activity, is a region that is particularly affected by LoL events. Upon examining the distribution of LoL events in relation to the various IMF orientations, we observe that the maximum relative to the cusp shifts toward dawn or dusk, depending on the sign of the IMF $B_y$ component. This phenomenon is evident in both hemispheres.

A magenta curve was added to each of the four polar maps in Figure 2, corresponding to the MLat value of 75°. This curve allows us to distinguish two distinct regions: one at higher latitude (MLat ≥ 75°), which includes the

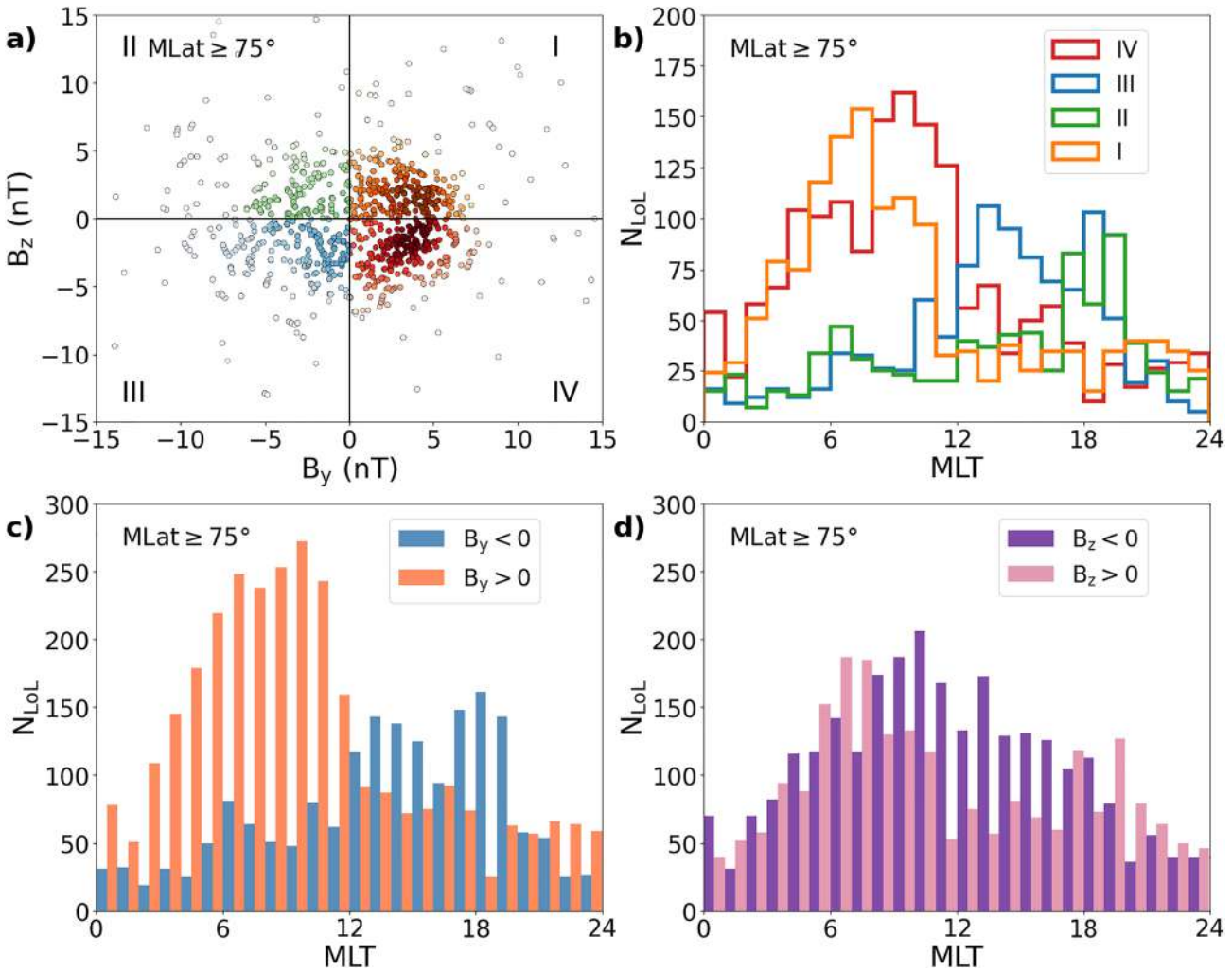


**Figure 3.** (a) Global Positioning System (GPS) loss of lock (LoL) events distribution at MLat ≥ 75° as a function of interplanetary magnetic field (IMF) $B_y$ and $B_z$ values. Different colors have been chosen for each sector and, within each sector, the intensity of the chosen color provides an indication of the number of events; (b) GPS LoL event distributions in each IMF sector as a function of MLT. The colors of the traces match those in the panel (a). (c) GPS LoL event distributions as a function of MLT, according to the different sign of the IMF $B_y$ component; (d) GPS LoL event distributions as a function of MLT, according to the different sign of the IMF $B_z$ component.

polar cusp and polar region, and one at a lower latitude (50° ≤ MLat < 75°), which essentially includes the auroral oval. This distinction is useful in comparing our results to previous studies that examined both polar caps and/or auroral ovals.

Figure 3 provides a detailed examination of GPS LoL events observed in the Northern hemisphere at high latitudes (MLat ≥ 75°) as a function of IMF orientation on the GMS yz-plane. This Figure 3 is composed of four panels, each describing different characteristics of the LoLs. Panel a shows the distribution of LoL events as a function of $B_y$ and $B_z$ values. Different colors have been assigned to each sector and the intensity of each color corresponds to the number of events. As the color intensifies, the number of LoL events linked to a given pair of IMF values increases. The majority of LoL events tend to cluster in the sector with $B_z < 0$ and $B_y > 0$, although even the sector with $B_z > 0$ and $B_y > 0$ has a significant number of events as seen in Figures 1 and 2. In panel b of Figure 3, we show how the number of LoLs recorded in each IMF sector varies with MLT. To more easily distinguish the trend of the number of LoLs with MLT for each IMF sector, the colors of the traces match those in panel a. According to the trends reported in panel b, the majority of LoL events takes place near the noon sector, confirming the cusp as the region most affected by LoL events. The events distribution is not symmetrical with respect to midday, but there is an excess of events in sectors 06:00–12:00 MLT, owing primarily to

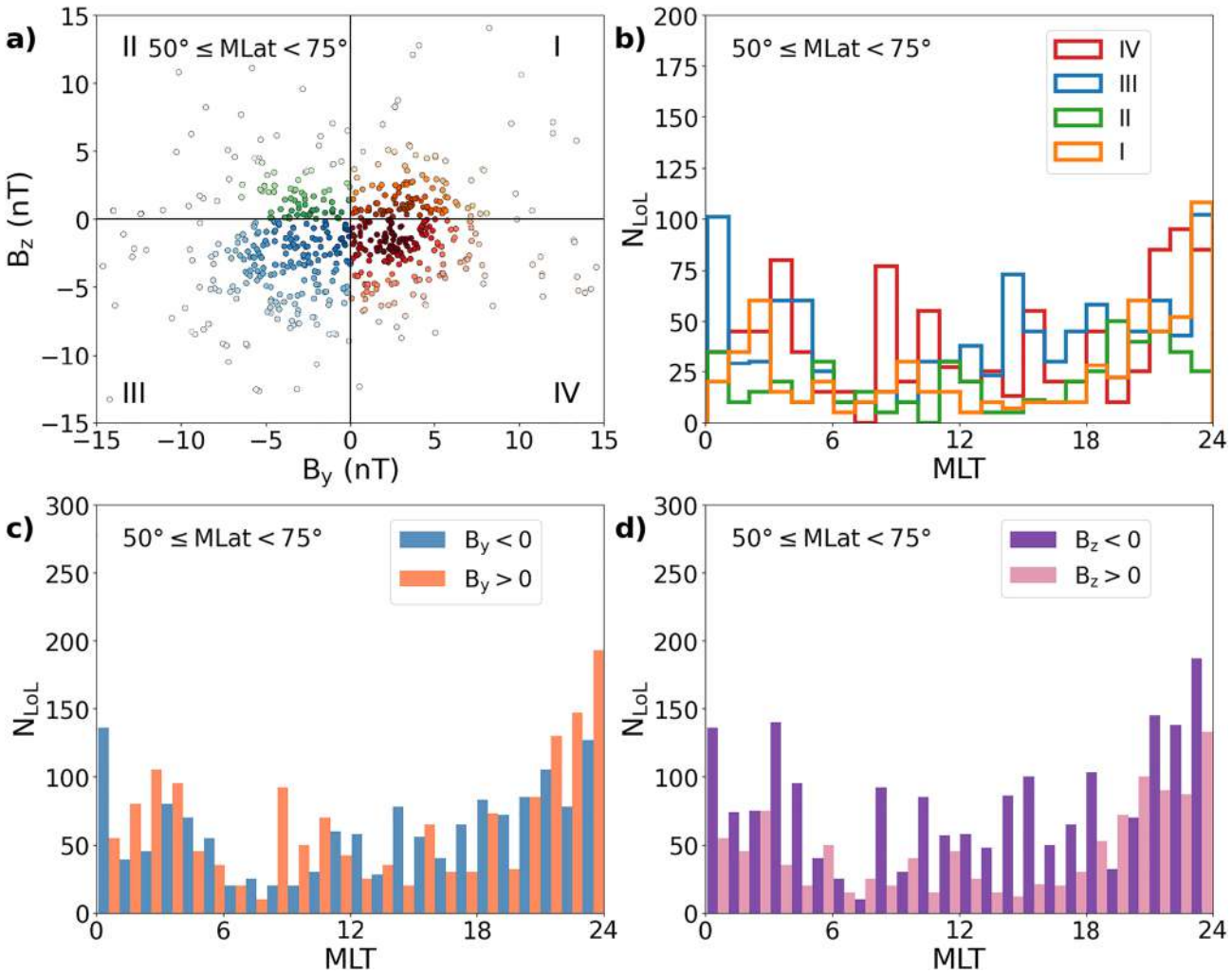


**Figure 4.** (a) Global Positioning System (GPS) loss of lock (LoL) events distribution at 50° ≤ MLat < 75° as a function of interplanetary magnetic field (IMF) $B_y$ and $B_z$ values. Different colors have been chosen for each sector and, within each sector, the intensity of the chosen color provides an indication of the number of events; (b): GPS LoL event distributions in each IMF sector as a function of magnetic local time (MLT). The colors of the traces match those in the panel (a). (c) GPS LoL event distributions as a function of MLT, according to the different sign of the IMF $B_y$ component; (d) GPS LoL event distributions as a function of MLT, according to the different sign of the IMF $B_z$ component.

events that occur in conjunction with $B_y > 0$. This trend is more pronounced in panel c of the same figure, where the number of LoL events is reported as a function of the sign of IMF $B_y$ component, once again as a function of MLT. When the IMF $B_y$ component is positive, LoL events tend to be concentrated at high latitudes in the midnight-dawn-noon sector. In panel d of Figure 3, we show the trend of the number of LoL events as a function of MLT, considering only the sign of the $B_z$ component. The plot clearly indicates a tendency for LoL events to cluster around midday and to increase in the case of a negative value of IMF $B_z$ component.

The same analysis was performed on the LoLs recorded in the auroral oval region (50° ≤ MLat < 75°). The results obtained from the analysis are presented in Figure 4. Panels a and b indicate that LoL events tend to occur more frequently for $B_z < 0$. The analysis of the MLT distribution reveals that LoLs tend to occur frequently at night, specifically between the hours after sunset and the early morning hours (18:00–03:00). Additionally, several LoL events are also observed around noon, which are associated with events occurring on the cusp and extending to magnetic latitudes below the 75° threshold set in our analysis. Unlike the patterns observed at higher latitudes, the LoL events at these latitudes do not exhibit a preferred MLT path as a function of the sign of $B_y$ or $B_z$ sign.

The same study was performed in the Southern hemisphere, where there are more LoL events (see Figure 5). Here the distributions are even clearer than those of the Northern Hemisphere. The shift of the concentration of

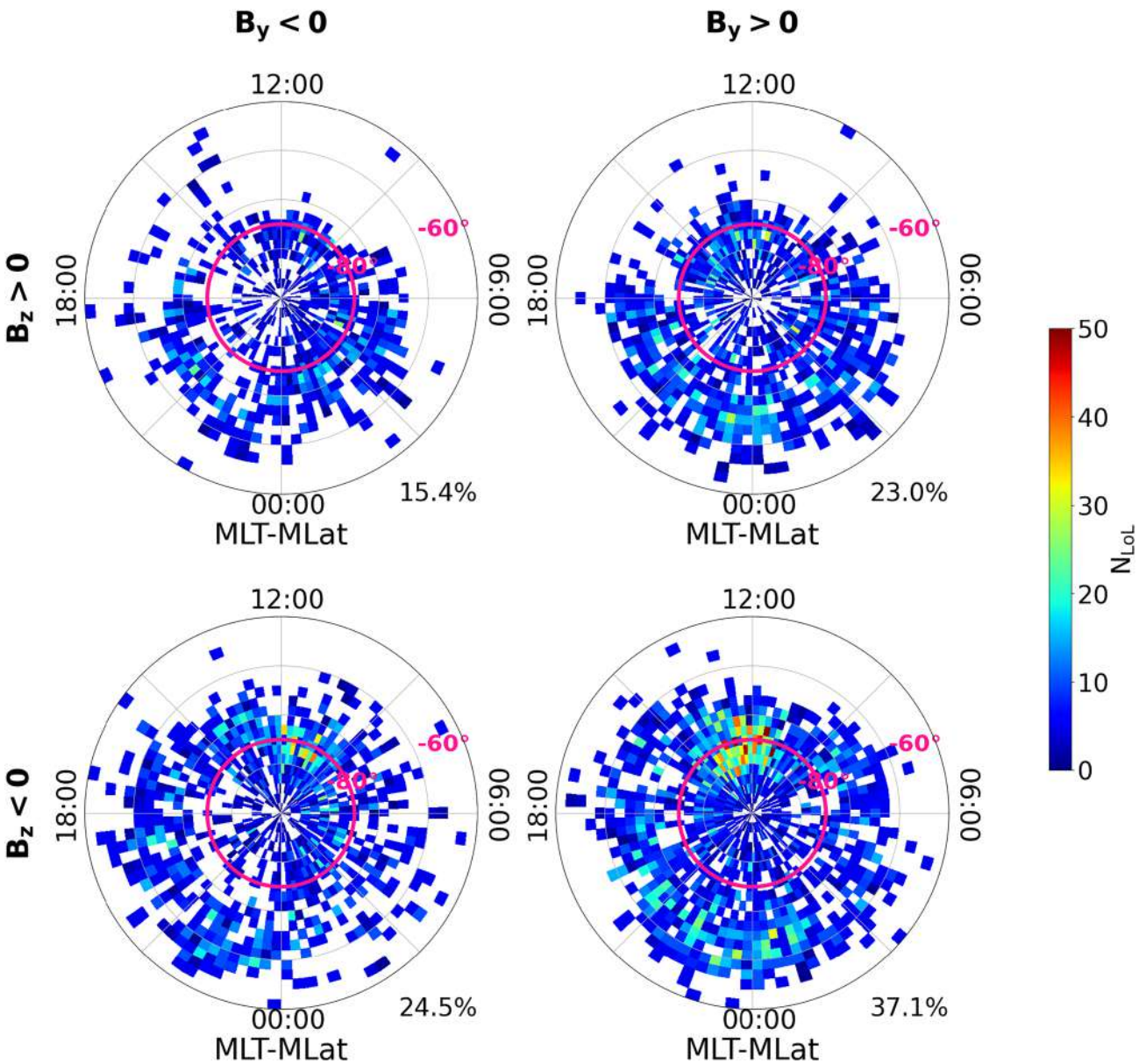


**Figure 5.** Polar view of loss of lock events spatial distribution for the Southern hemisphere in a quasi-dipole magnetic latitude (MLat ≤ −50°N) and magnetic local time reference frame, for four different interplanetary magnetic field (IMF) sectors in the geocentric solar magnetospheric yz-plane. Maps have been drawn using data recorded onboard Swarm A and Swarm B from 15 April 2014 to 31 December 2021. MLat = −75°N can be distinguished by the magenta colored curve. Percentage at bottom right of each plot indicates the fraction of events characterized by that particular IMF configuration, with respect to the total number of events.

events in the cusp region toward dawn or dusk depending on IMF $B_y$ sign, previously mentioned, is also visible here. However, the shift is reversed compared to the one seen in Figure 2 because $B_y$'s effect is mirrored in the two hemispheres. Additionally, the maxima in the cusp are more distinct when $B_z < 0$. Because there are more events in this hemisphere, it is easier to observe another interesting characteristic: LoL events spread over a larger area during negative $B_z$ periods, reaching lower magnetic latitudes than during positive $B_z$ periods. Moreover, LoLs appear to be favored by a positive configuration of the IMF field's $B_y$ component, particularly between 21:00 and 01:00 MLT, at lower latitudes. These features are evident in the results presented in Figures 6 and 7. We analyzed the dependence of LoLs on IMF orientation in the Southern hemisphere in the same way as in the Northern hemisphere, considering the events occurring at magnetic latitudes greater and less than −75°.

Figure 6 presents a detailed analysis of the LoL events observed at high latitudes (MLat ≤ −75°) in relation to the IMF orientation on the GSM yz-plane. Panel a shows the distribution of LoL events as a function of $B_y$ and

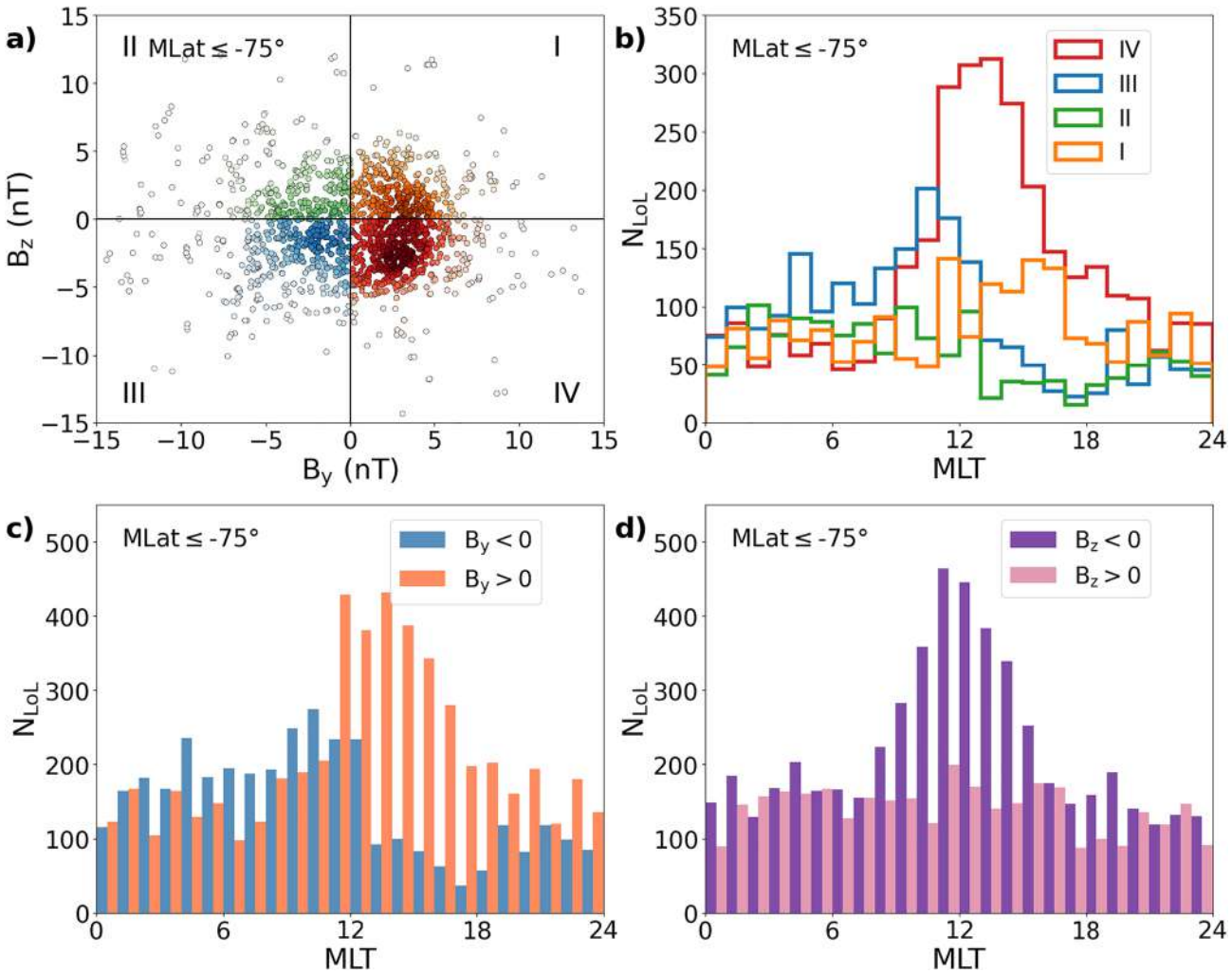


**Figure 6.** (a) Global Positioning System (GPS) loss of lock (LoL) events distribution at MLat ≤ −75° as a function of interplanetary magnetic field (IMF) $B_y$ and $B_z$ values. Different colors have been chosen for each sector and, within each sector, the intensity of the chosen color provides an indication of the number of events; (b) GPS LoL event distributions in each IMF sector as a function of MLT. The colors of the traces match those in the panel (a). (c) GPS LoL event distributions as a function of MLT, according to the different sign of the IMF $B_y$ component; (d) GPS LoL event distributions as a function of MLT, according to the different sign of the IMF $B_z$ component.

$B_z$ values, indicating that the majority of LoL events cluster in the sector with $B_z < 0$ and $B_y > 0$. In panel b, the number of LoLs recorded in each sector is plotted as a function of MLT, revealing that most LoL events occur close to noon, confirming the cusp as the area with the highest number of LoL events. The LoL distribution is not symmetric with respect to noon, with more events occurring in the time periods between 12:00 and 18:00 MLT due to events that coincide with IMF characterized by $B_y > 0$. This trend is more apparent in panel c, where the number of LoL events is shown as a function of the sign of the IMF $B_y$ component, and then as a function of MLT. Here, LoL events tend to concentrate at high latitudes in the midnight-dusk-noon sector when the IMF $B_y$ component is positive. Finally, in panel d, the trend of the number of LoL events as a function of the MLT is reported in the panel d, taking only the sign of IMF $B_z$ component into account. This plot clearly shows that LoL events tend to increase with negative values of $B_z$ and cluster around noon.

Figure 7 displays the LoL distributions in the area enclosed by the coordinates −75° < MLat ≤ −50°, yielding results similar to Figure 4. The early morning and late evening distribution peaks, which correspond to the events occurring in the night-side auroral oval, are even more distinct in this instance. Panel c of Figure 7 confirms that $B_y > 0$ is the most favorable condition for LoL occurrence in the nightside auroral oval region. Additionally, both $B_z$ orientations contribute equally during the night; around noon, the peak corresponding to the cusp's lower latitudes, which is favored by negative $B_z$ conditions, can be observed once again.

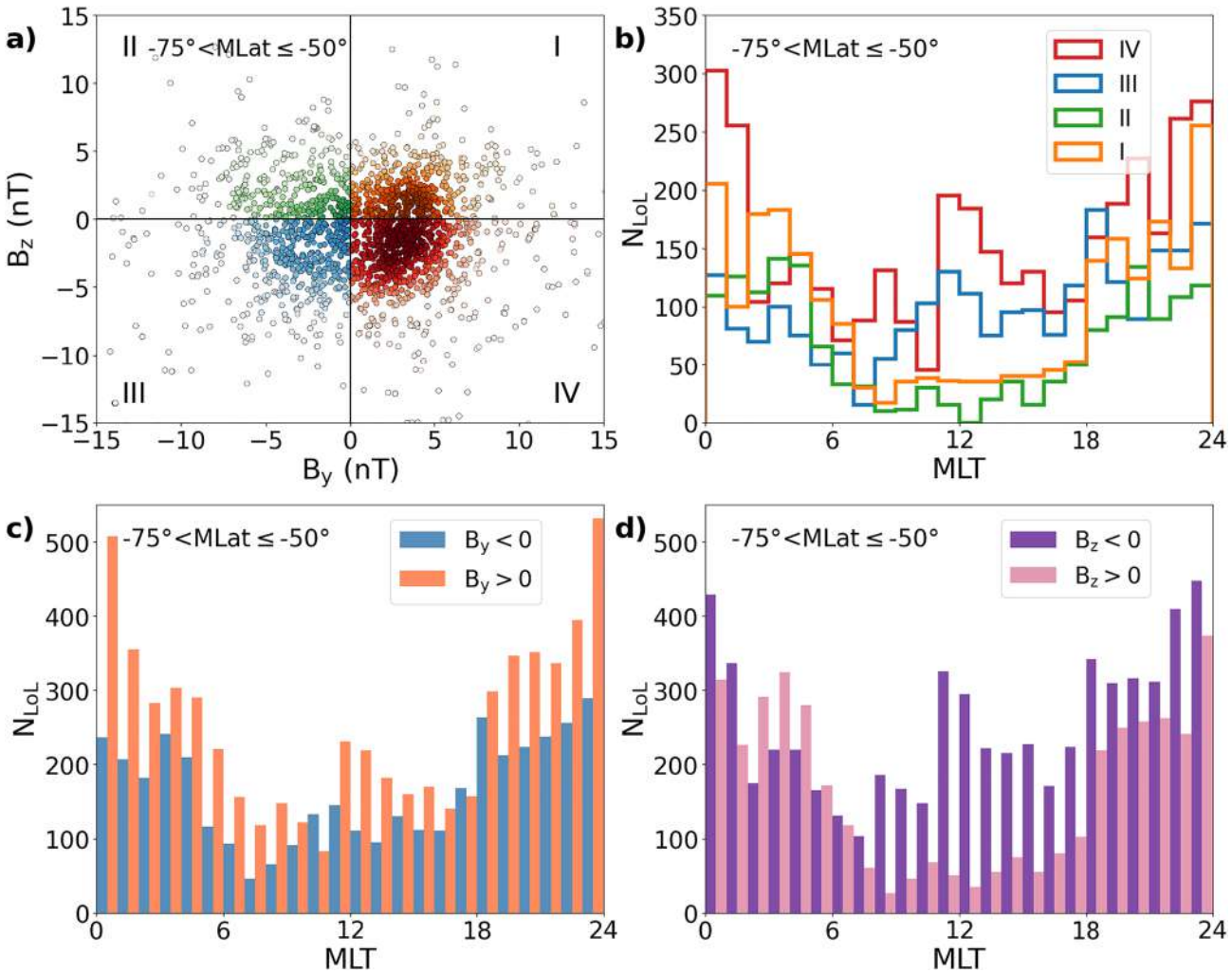


**Figure 7.** (a): Global Positioning System (GPS) loss of lock (LoL) events distribution at $-75° < \text{MLat} \leq -50°$ as a function of interplanetary magnetic field (IMF) $B_y$ and $B_z$ values. Different colors have been chosen for each sector and, within each sector, the intensity of the chosen color provides an indication of the number of events; (b) GPS LoL event distributions in each IMF sector as a function of MLT. The colors of the traces match those in the panel (a). (c) GPS LoL event distributions as a function of MLT, according to the different sign of the IMF $B_y$ component; (d) GPS LoL event distributions as a function of MLT, according to the different sign of the IMF $B_z$ component.

We looked also for any possible correlation between the LoL event's duration and the related IMF conditions. To achieve this result, we examined the cumulative distribution of LoL duration, considering both the hemispheres together, and divided the events into three different groups of increasing duration. We specifically identified three groups by taking into account the distinctive shape of the cumulative distribution (see Figure 8 on the left), which is characterized by an extremely high number of LoL events with a time duration ($\Delta T$) of about 18/19 s, as also found by Xiong et al. (2018). By setting two thresholds in the cumulative distribution at approximately 9% and 78%, we divided the events into those with $\Delta T < 18$ s, those with $18 \text{ s} \leq \Delta T \leq 19$ s, and those with $\Delta T > 19$ s. By averaging the $B_y$ and $B_z$ components in relation to the events that make up each group, we were able to create an associated vector in the yz-plane. Figure 8 reports the cumulative distribution of LoL duration on the left, with the resulting IMF vectors in the yz-plane on the right. Vectors are colored according to the LoLs' group they refer to. According to what is shown in the upper right plot of Figure 1, all three vectors in both hemispheres are located in the IV sector. It's worth noting that the green and the orange vectors, which represent the groups of events with the shortest and longest duration respectively, have similar module. The purple vector, representing approximately 70% of the events, which lasted 18 or 19 s, is associated with a lower IMF intensity in the yz-plane.

As it was evident from the previous analysis, IMF orientation, which is in charge of plasma motions in the high latitude ionosphere, has an impact on GPS LoL events. By using the electrostatic potential maps obtained from

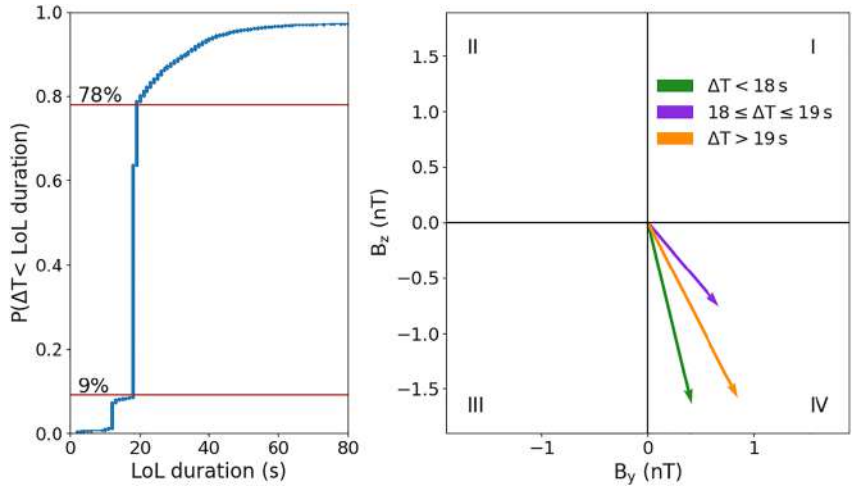


**Figure 8.** On the left is the cumulative distribution of loss of lock (LoL) duration, with two horizontal red lines representing the two $\Delta T$ threshold values that classified LoLs into one of three groups. The mean interplanetary magnetic field (IMF) vector projections in the yz-plane are shown on the right. Each vector is constructed by taking into account the IMF values associated with a specific class of LoL events. The green vector represents all LoL events that last less than 18 s. The purple vector corresponds to events with 18 s $\leq \Delta T \leq$ 19 s. Finally, the orange vector is obtained by taking into account the longest events ($\Delta T >$ 19 s). This diagram combines events that occur in both hemispheres.

the empirical convection model based on the high-frequency coherent scatter radars of the Super DualAuroral Radar Network (SuperDARN) data, we compared the spatial distribution of LoL events on MLat—MLT plane to the high-latitude convective cells (Chisham et al., 2007). SuperDARN consists of high-frequency (8–20 MHz) coherent scatter radars, which emit a series of radio wave pulses that are transmitted in a beam forward of the antenna arrays. In this way it is possible to measure the velocity of the ionospheric convection flow in the radar look direction over the polar regions and obtain information on the decameter-scale plasma irregularities in the *E* and *F* regions of the ionosphere by measuring the Doppler shift between the transmitted signal and the reflected one. By combining the line-of-sight vectors from various radars with overlapping fields of view, the radar observations can cover a wide area and provide a thorough understanding of the motion of plasma in the polar ionosphere. We use the "map potential" model developed by Ruohoniemi and Baker (1998), which combines data from a statistical model (Ruohoniemi & Greenwald, 1996) to produce a convection pattern over the entire convection zone that is in the best agreement with the line-of-sight velocity measurements provided by the SuperDARN radars. This model, known as the CS10, can reproduce the mesoscale features of ionospheric convection patterns at high latitudes for a wide range of solar wind, IMF, and dipole tilt angle parameter values. Thus, for each of the four possible IMF orientations in the GSM yz-plane, we generated an average pattern of the high-latitude ionospheric convection pattern. Each pattern is obtained considering as input data the root mean squared values of $B_z$, $B_y$, and solar wind velocity obtained from OMNI data in the periods associated with the occurrence of LoL events, in each selected IMF sector and setting the dipole tilt angle to $-10°$ for Northern hemisphere and 10° for Southern hemisphere. Because LoL events typically occur more frequently between September and May, they are centered on either local winter or local summer conditions depending on the hemisphere, which is why these values for the dipole tilt angle were chosen. Data so generated have been downloaded from the SuperDARN Dynamic Model Web Interface (http://sdnet.thayer.dartmouth.edu/models/dynamicmodel.php#SDDM). Figure 9 displays the electrostatic potential maps generated using the empirical convection model based on SuperDARN data and the LoL events in the Northern hemisphere, on the MLat—MLT plane, recorded by Swarm satellites. It is interesting to note that the LoL events that occur at the cusp and over the polar cap preferentially appear in the space between the two cells, following the plasma motion trajectory toward the night-side, especially when the IMF $B_y$ component is positive. The events that make up the night-side band, on the other hand, typically occur at the edge of convective cells, where the flow begins to turn back toward the Sun, moving from lower latitudes in the dawn and dusk sectors. A similar pattern can be seen in the Southern Hemisphere, as shown in Figure 10.

We repeated the previous analysis by considering different IMF orientations in the GSM xy-plane. This was done to investigate whether there was a specific effect associated with the IMF $B_x$ component. Here we show the results only for the Southern hemisphere, where the higher number of events provides clearer insights into their

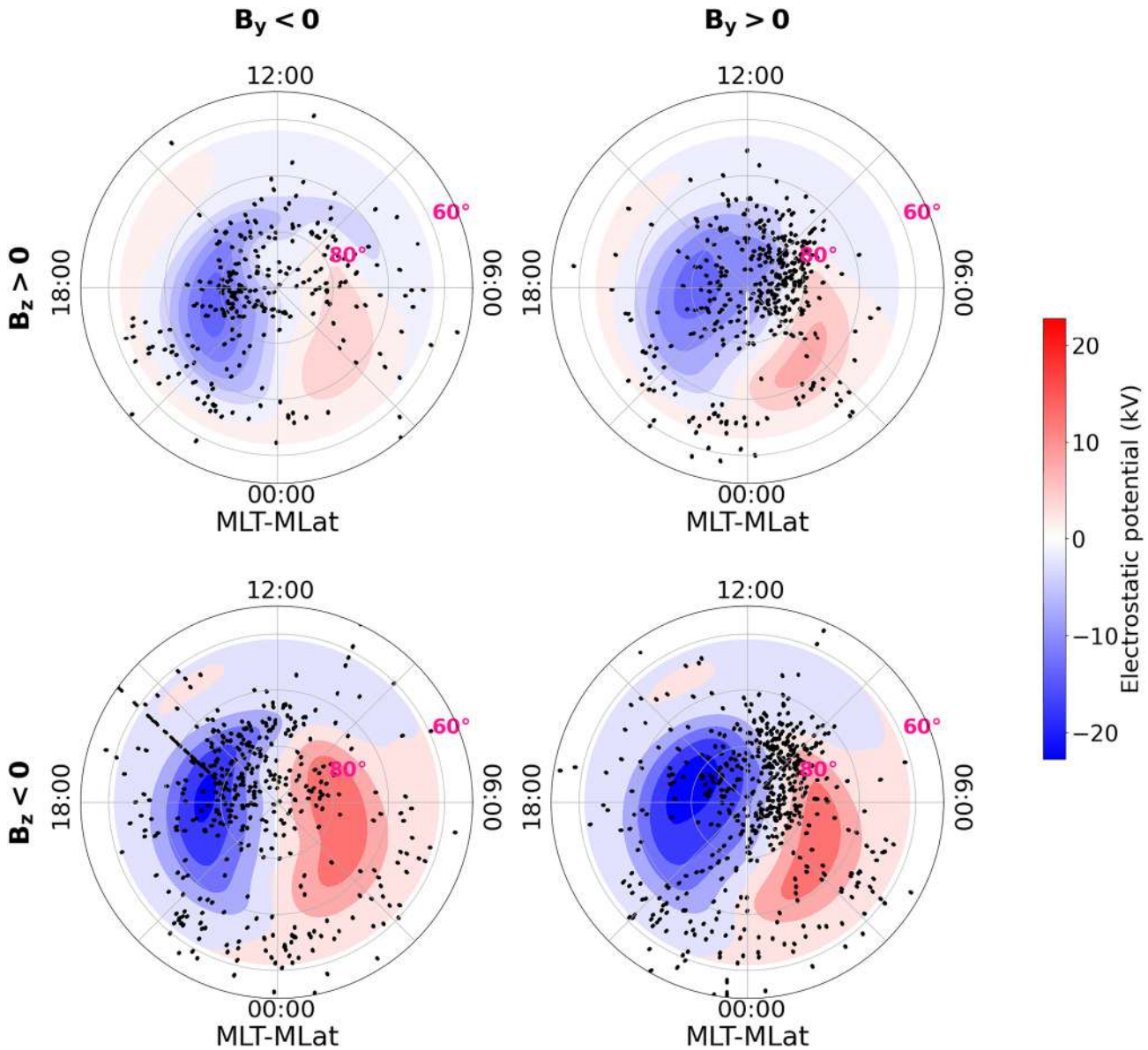


**Figure 9.** Comparison between Global Positioning System loss of lock (LoL) events recorded by Swarm constellation and SuperDARN polar potential maps obtained using the statistical convection model CS10. Data are reported as a function of magnetic local time and magnetic latitude in the Northern hemisphere according to different interplanetary magnetic field (IMF) orientations in the geocentric solar magnetospheric yz-plane. Color is used to represent electrostatic potential using the scale on the right. A black dot is used to represent each LoL event that happened under that IMF conditions.

characteristics. However, the results in the Northern hemisphere are comparable. Figure 11 represents the GPS LoL events spatial distribution at mid and high latitude, depending on the $B_x$ and $B_y$ signs. As one can see, the configurations with the highest number of GPS LoLs are those in which the signs of the $B_x$ and $B_y$ components are opposite. This reflects the anti-correlation between these two components, which was already observed when looking at their joint PDF (see Figure 1's second row) and that is due to the spiral structure of the IMF. The configuration with negative values of the IMF $B_x$ component and positive values of the IMF $B_y$ component is more favorable to the occurrence of GPS LoLs, hosting nearly half of the total number of events. The effect of the IMF $B_x$ component on the spatial distribution of GPS LoLs appears to be similar to that of the IMF $B_y$ component in the GSM yz-plane. In fact, as shown in our analysis of the Southern hemisphere (results in the Northern hemisphere are comparable), the events in the cusp region shift from dawn to dusk when the $B_x$ component changes from positive to negative values. The effects of IMF $B_x$ on the spatial distribution of GPS LoLs are similar to those of IMF $B_y$ in the GSM yz-plane, as shown in Figure 12. This figure presents the LoL events observed at

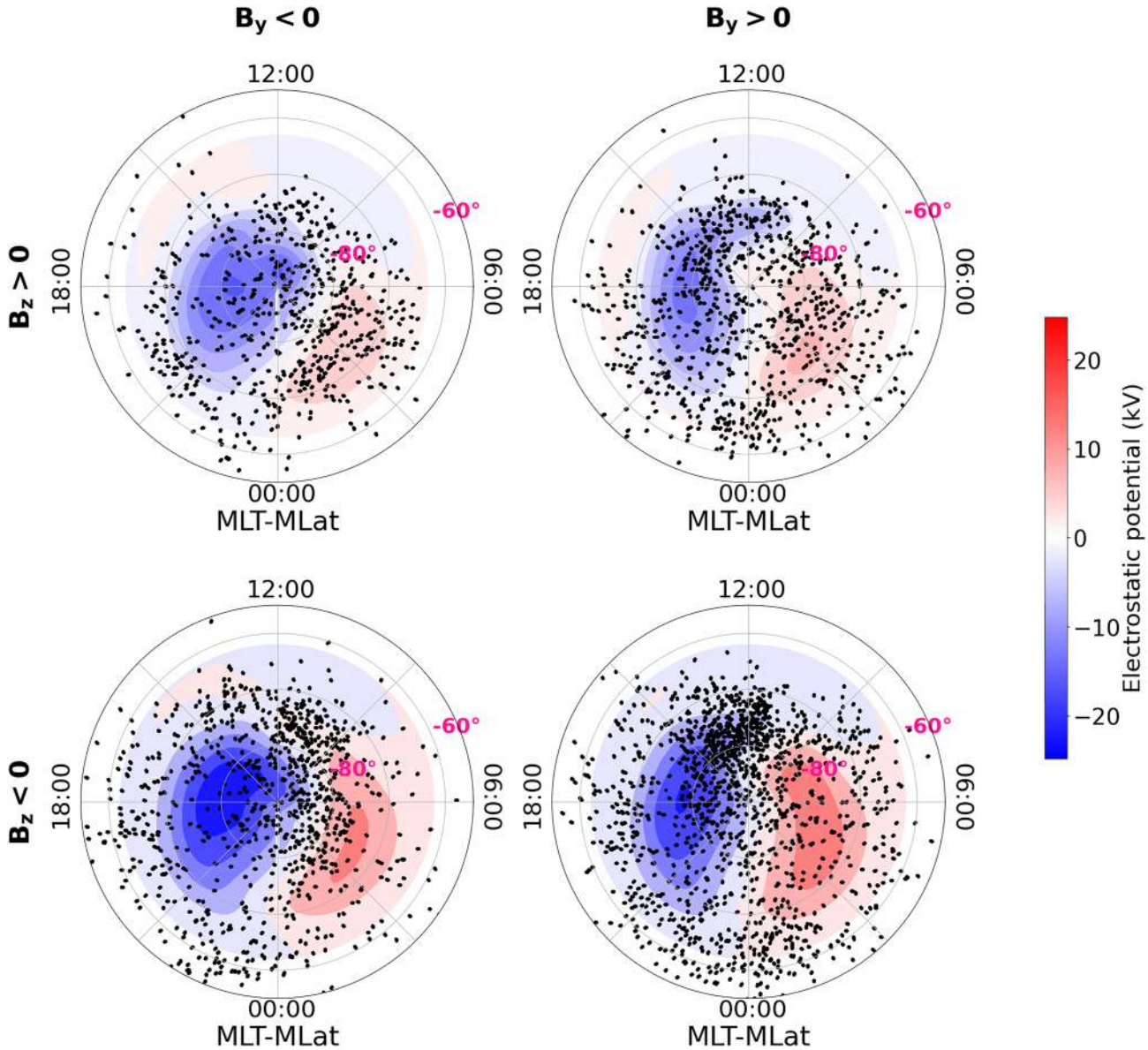


**Figure 10.** Comparison between Global Positioning System loss of lock (LoL) events recorded by Swarm constellation and SuperDARN polar potential maps obtained using the statistical convection model CS10. Data are reported as a function of magnetic local time and magnetic latitude in the Southern hemisphere according to different interplanetary magnetic field (IMF) orientations in the geocentric solar magnetospheric yz-plane. Color is used to represent electrostatic potential using the scale on the right. A black dot is used to represent each LoL event that happened under that IMF conditions.

high latitudes (MLat $\leq -75°$), as a function of MLT and IMF orientation on the GSM xy-plane. Panel a displays the distribution of LoL events as a function of $B_x$ and $B_y$ values, with most events concentrated in the II sector. The associated distribution of LoL events as a function of MLT is shown in green in panel b, and it reveals a peak shifted toward the afternoon hours rather than being centered around noon. The most intriguing findings are presented in panels c and d of the Figure, where the GPS LoLs distribution is reported as a function of MLT taking into account the sign of the IMF $B_x$ and $B_y$ components, respectively. The results obtained for the latitude band $-75° <$ MLat $\leq -50°$ are analogous and, therefore, not shown.

## 4. Discussion and Conclusions

This paper builds on the observation that GPS LoL events are frequently caused by ionospheric irregularities, whose formation and behavior depend on various factors. Previous studies aimed identifying the physical causes

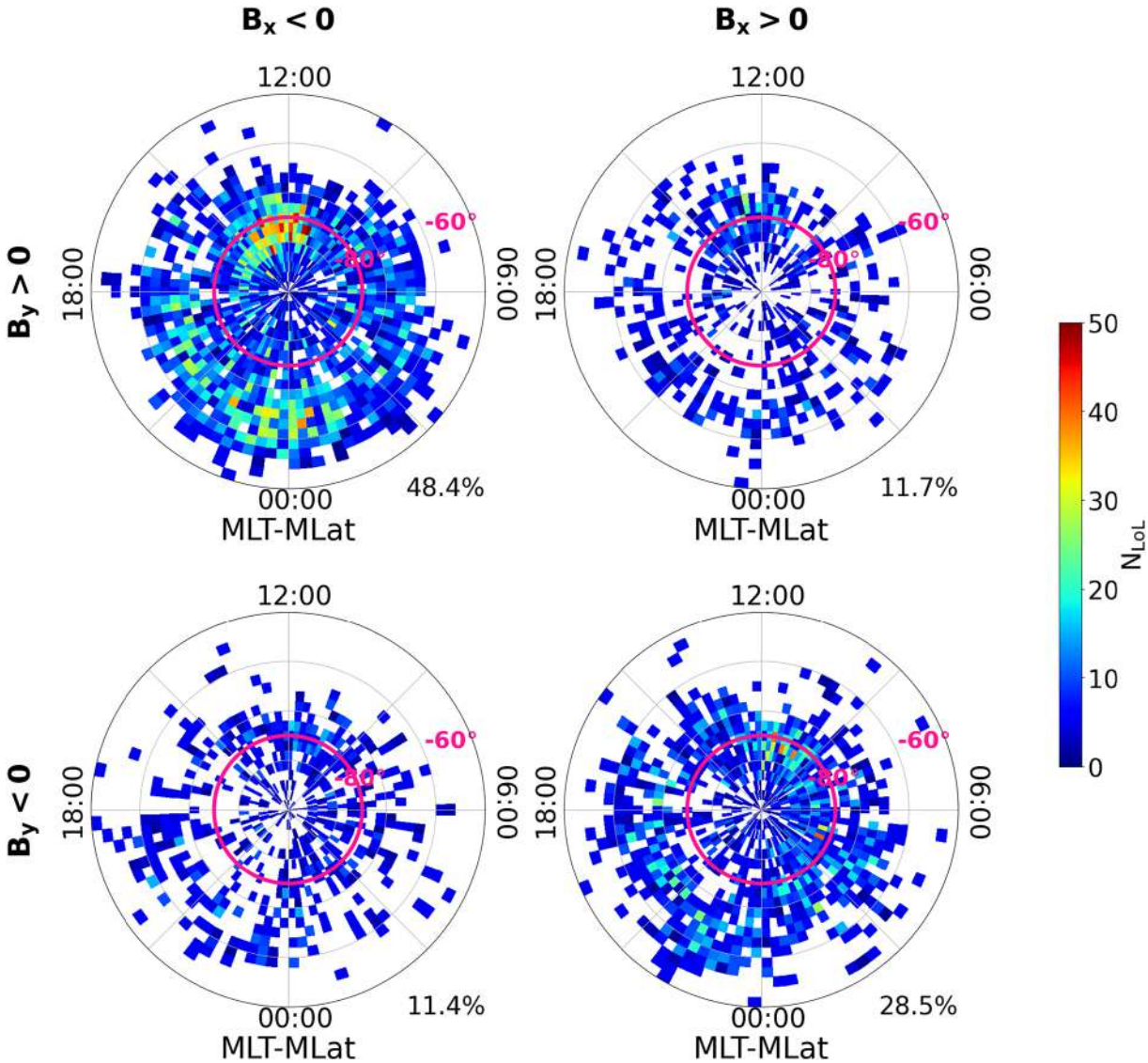


**Figure 11.** Polar view of loss of lock events spatial distribution for the Northern hemisphere in a quasi-dipole magnetic latitude (MLat ≥ 50°N) and magnetic local time reference frame, for four different interplanetary magnetic field (IMF) sectors in the geocentric solar magnetospheric xy-plane. Maps have been drawn using data recorded onboard Swarm A and Swarm B from 15 April 2014 to 31 December 2021. MLat = 75°N can be distinguished by the magenta colored curve. Percentage at bottom right of each plot indicates the fraction of events characterized by that particular IMF configuration, with respect to the total number of events.

underlying ionospheric irregularities formation, and the processes that affect their presence and spatiotemporal distribution. Theoretical studies and simulations have addressed different instability processes, while analyses of their distribution based on MLat, MLT, season, geomagnetic conditions and solar activity have been conducted. Given that Pezzopane et al. (2021) have already examined the dependence of GPS LoLs on MLat, MLT, season, and solar activity, we decided to investigate the impact on these events of another parameter, which had not yet been taken into account: the IMF orientation. We focused on the high-latitude regions, where the IMF has a strong influence on the ionospheric plasma dynamics. We analyzed GPS LoL events recorded by the Swarm constellation between 15 July 2014, and 31 December 2021. We assigned to each LoL event a mean value of the IMF's $B_x$, $B_y$, and $B_z$ components, consistent with the average values of the IMF 20–40 min prior to the LoL event. Subsequently, we grouped the LoL events based on their relative IMF orientation in the GSM yz- and xy- planes and examined how their distributions in QD MLat and MLT vary with respect to the IMF orientation. In order to determine whether specific IMF orientations are associated with the occurrence of LoL events, we first looked at the joint PDF between the $B_y$ and $B_z$ component values for the entire chosen time period. We then compared the results to the PDF of the $B_y$ and $B_z$ values conditioned on the occurrence of GPS LoL events. Following that, we

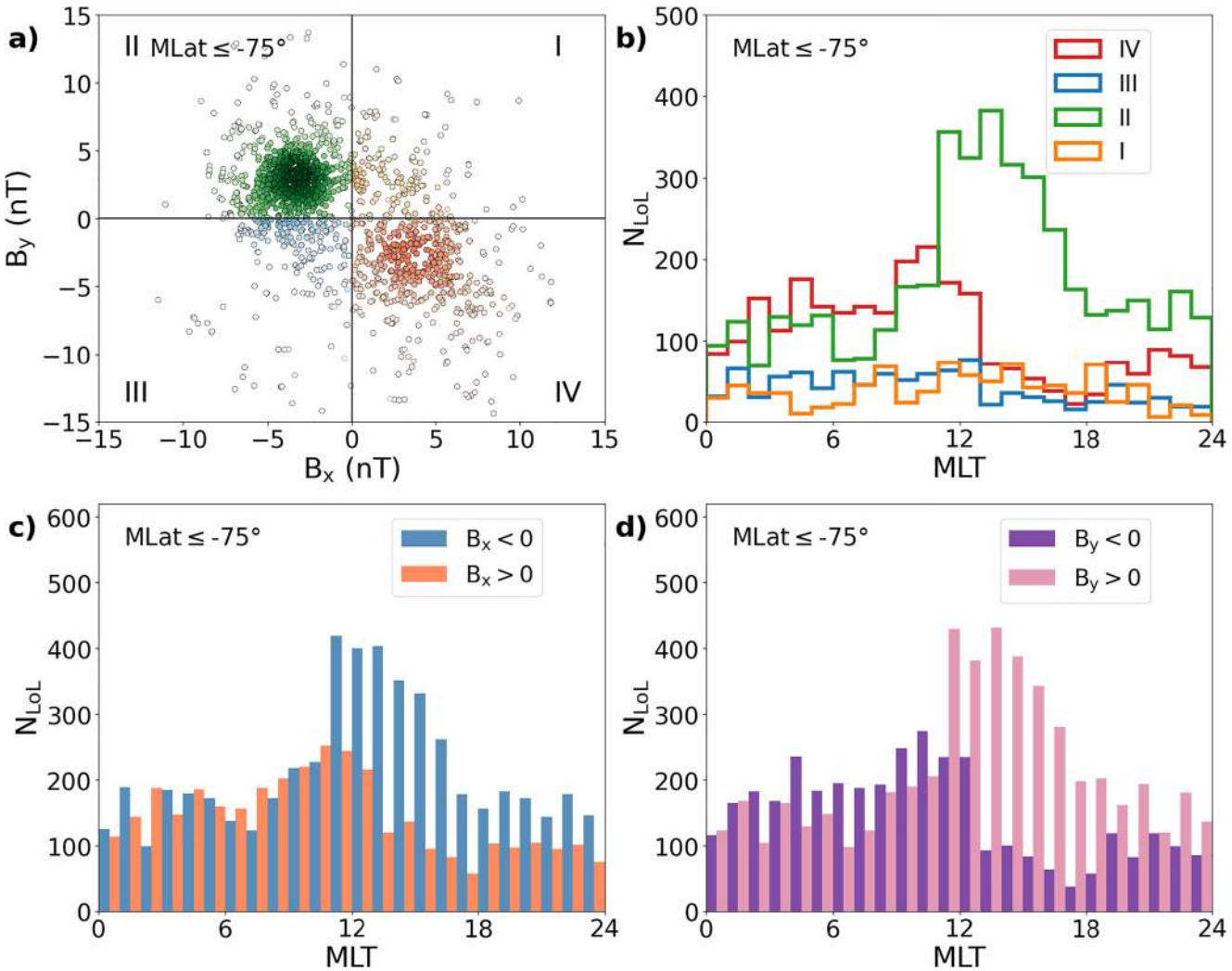


**Figure 12.** (a): Global Positioning System (GPS) loss of lock (LoL) events, occurred at MLat ≤ −75°, are represented by circles colored according to the interplanetary magnetic field (IMF) sector in geocentric solar magnetospheric xy-plane they belong to. Darker color indicates higher grouping of points; (b) GPS LoL event distributions in each IMF sector as a function of magnetic local time (MLT). The colors of the traces match those in the panel (a). (c) Distributions of GPS LoL events as a function of MLT and with respect to the IMF $B_x$ component sign; (d) Distributions of GPS LoL events as a function of MLT and with respect to the IMF $B_y$ component sign.

also compared the PDF of the $B_x$ and $B_y$ values conditioned on the occurrence of GPS LoL events with the PDF of the $B_x$ and $B_y$ values over the entire selected time period. The results of these comparisons are shown in Figure 1 and it is immediately obvious that the LoL events seem to happen more frequently when the IMF is oriented in a particular way. In fact, the traditional distribution of the values in the GSM yz-plane, characterized by two main peaks in almost exclusively eastward and westward directions (Haaland et al., 2007), is detectable by examining the PDF of the $B_y$ and $B_z$ values associated with the entire chosen period, which reflects the IMF orientation along the Parker spiral. On the same plane, the PDF of the $B_y$ and $B_z$ values conditioned to the occurrence of LoL events has a completely different distribution. LoL events are favored by a specific range of IMF clock-angle in the GSM yz-plane, which includes the IV sector ($B_y > 0$, $B_z < 0$) in particular, but also a portion of the I sector ($B_y > 0$, $B_z > 0$). The IV sector implies negative $B_z$ values, which enhance magnetic reconnection at the low-latitude dayside magnetopause, strongly influencing plasma motions in the polar regions with the formation of the two large-scale convective cells. The $B_y$ sign, on the other hand, influences the location and shape of the cells. The most advantageous condition appears to be $B_y > 0$. This is also visible in the right panel of the second row of Figure 1, where the PDF of $B_x$ and $B_y$ values conditioned on LoL events is reported. Even on the GSM xy-plane, an IMF orientation with a positive $B_y$ component and a negative $B_x$ component seems to favor the occurrence of LoL events.

Figures 2 and 5 represent the polar views of LoL events distribution in QD MLat and MLT, depending on IMF orientations in the GSM yz-plane, for Northern and Southern hemispheres, respectively. The shift in MLT of the location of the maximum of LoL events, which is visible at high latitude around noon, is a significant feature that can be seen in both hemispheres. This maximum relates to the cusp region, where particle precipitation may result in the development of irregularities of plasma density, which may result in LoL events. The IMF $B_y$ component sign is clearly a factor in determining where this maximum is located. The maximum for positive values of the IMF $B_y$ component, which is always around noon, tends to move toward dawn in the Northern hemisphere and toward dusk in the Southern one. In the case of a negative value for the IMF $B_y$ component, the maximum moves in the opposite direction. This movement of the maximum of LoL events around noon at high latitude corresponds with the movement of the cusp region as a function of IMF $B_y$ sign (Tanaka, 2007). This feature is also visible in Figures 3 and 6, where panel c reports the LoLs' MLT dependence, conditioned to the sign of $B_y$, at those latitudes ($|\text{MLat}| \geq 75°$), which roughly include the cusp and the polar cap. This feature is consistent with recent findings regarding the dependence of polar cap patches on the sign of the IMF $B_y$ component (Spicher et al., 2017). The polar cap patches are plasma density enhancements caused by the segmentation of the ionization tongue, whose triggering mechanism is still debated (Clausen & Moen, 2015). Once formed, plasma convection transports them over the polar cap. When sorted by IMF $B_y$ sign, their spatial distribution is characterized by a dawn-dusk asymmetry, with a higher number found in the Northern postnoon and prenoon sectors for negative and positive IMF $B_y$ components, respectively. The phenomenon has an interhemispheric asymmetry. The strong correlation between the characteristics of polar cap patches and LoL events suggests that these plasma density irregularities may be a cause of LoL events. This hypothesis is supported also by Cherniak and Zakharenkova (2016) and Xiong et al. (2019), who both investigated the effect of polar cap patches formed during the 2015 St. Patrick's Day storm on the GPS receivers onboard Swarm A and B. They discovered that both satellites lost contact with several GPSs while crossing different patches. In particular, Xiong et al. (2019) looked into why Swarm B lost GPS signal on all eight channels but Swarm A only on four, despite passing through polar patches with comparable magnitudes of dense plasma and taking into account that satellites at lower altitudes are typically more affected by LoL events. The impact on GPS signal, according to the justification provided, is also dependent on where the polar cap patches are located. Swarm B encountered a patch near the cusp, where they become more structured and are accompanied by a number of instabilities. Patches become less organized and have less impact on the GPS signal after the polar cap's plasma convection. Focusing on the effect of $B_z$ in Figures 2 and 5, we can see that the majority of events in both hemispheres take place when this component is negative, which occurs when there is a magnetic reconnection at the dayside magnetopause. In this configuration of the IMF, the two cells pattern covers a larger area and descends to lower latitudes, resulting in a higher rate of open flux in the magnetosphere and more efficient convection of the high-latitude plasma. In fact, LoL events associated with $B_z < 0$ are distributed over a wider region, both on the dayside and on the nightside, as it is particularly noticeable in the Southern hemisphere. Now, if we focus on the QD MLat band that includes the nightside auroral oval region ($50° \leq |\text{MLat}| < 75°$), we can see from Figures 4 and 7 that the IMF $B_y$ and $B_z$ influence on LoLs' MLT coordinate is not straightforward. The only clear feature is a generally higher number of events coinciding with $B_y > 0$ condition in the Southern hemisphere (see panel c of Figure 7). Then, excluding the events happening in the daily hours, which are dominated by the already described behavior followed by the cusp's lower part, the events occurring in the night sector do not show a clear MLT dependence on the IMF $B_y$ and $B_z$ components. We wanted also to verify if the IMF orientations had any effect on the duration of a LoL event. To do this, after examining the distinctive shape of the LoLs duration cumulative distribution, we divided the events into three groups based on their duration and calculated the mean $B_y$ and $B_z$ components for each group. As it was shown in Figure 8, all three obtained vectors lie on the IV sector of the yz-plane. This is consistent with the PDF of $B_y$-$B_z$ values conditioned on the occurrence of LoL events (see Figure 1), confirming that this type of event is favored by a particular IMF orientation. Furthermore, the shortest and longest events appear to be linked to a higher module of the IMF projection on the yz-plane, with respect of the events with duration equal to 18 or 19 s. What was discovered is difficult to understand. However, it appears that there is no correlation between the duration of LoL events and the IMF's strength, as the strength field is associated with LoLs of both extremely short and longer duration.

Next, we investigate the geographic position of the identified LoL events in relation to high-latitude convective cells. The distribution of these events, depicted as black points in Figures 9 and 10, can be seen in relation to SuperDARN polar potential maps, which were obtained using the statistical convection model CS10. The shape of the dayside cells determines where LoLs cluster, and then they move along the path between the two cells

toward the nightside sector. The events in the nighside band seem to take place in areas where the convective pattern is characterized by a return flow toward the Sun. This specific spatial location of the LoLs is clearer for conditions where $B_y > 0$ in the Northern hemisphere (see Figure 9) and $B_z < 0$ in the Southern hemisphere (see Figure 10). However, the behavior of LoLs is unclear in the remaining cases, although a preference for LoL distribution along the edges of convection cells is observed in all cases. Each SuperDARN map was created by taking the average value of the $B_y$, $B_z$, and solar wind velocity parameters and combining them with all of the LoL events from that specific IMF clock-angle sector. As a result, each LoL event may be better represented by a map generated using its own unique interplanetary conditions. Last but not least, focusing on the potential contribution of $B_x$ to the high-latitude dynamics that generates favorable conditions for LoL events, we found that its impact is correlated with $B_y$ due to the anti-correlation between these two parameters, which is brought about by the IMF spiral structure. In fact, we found that the effect of the $B_x$ sign usually corresponds to the effect of the opposite sign of $B_y$. There is a portion of LoL events for both the Northern (which is not displayed in this work) and Southern hemispheres that is roughly 20% of the total and corresponds to the case where $B_x$ and $B_y$ have the same sign. Even though the number of events in this case is insufficient to result in distinct features on the MLat-MLT maps, they are significant enough to deserve further investigation.

To summarize, our analysis of GPS LoL events recorded by Swarm satellites between 15 July 2014 and 31 December 2021, clearly indicates a dependence on the IMF orientation. These events occur more frequently when $B_z < 0$ and $B_y > 0$ and their spatial distribution in the QD-magnetic latitude and MLT coordinate systems is affected by the signs of $B_y$ and $B_z$, with the cusp and polar cap regions showing the strongest effects. This interplanetary influence highlights the connection between GPS LoL events and the high-latitude convection pattern. It is interesting to note that these events often occur in regions with ionospheric irregularities, primarily related to the occurrence of instabilities such as the gradient-drift instability, which arises from the interaction between plasma density gradients and electric fields, the Kelvin-Helmholtz instability, which arises from the shear between plasma flows with different velocities, and the current-convective instability, caused by a turbulent heating of the plasma due to the passage of a current. All of these instabilities typically take place in the cusp, in the auroral oval, and near the dawn and dusk terminators (Greenwald et al., 2002). These instabilities can also lead to the development of a turbulent regime in the plasma. Recently, it has been shown (De Michelis et al., 2022) that LoL events tend to occur at high latitudes in the presence of electron density fluctuations in a turbulent regime, characterized by extremely high values of the RODI index, which is a proxy of the rate of change of electron density in the ionosphere. The findings of this work confirm the importance of the presence of electron density fluctuations with specific properties as a necessary condition for the occurrence of a possible LoL event. These results are part of a better understanding of the mechanisms and triggering factors of LoLs, which is helpful in assessing the risk of this phenomenon and mitigating its effects on GNSS systems.

## Data Availability Statement

The results presented rely on data collected by ESA-Swarm mission (ESA, 2022). We thank the European Space Agency that supports the Swarm mission. Swarm data can be accessed at ftp://swarm-diss.eo.esa.int. IMF components and solar wind velocity data were downloaded from OMNIWeb Data Explorer website (https://omniweb.gsfc.nasa.gov/form/dx1.html), operated by the Goddard Space Flight Center (NASA) Space Physics Data Facility (NASA, 2022). We also acknowledge the national scientific funding agencies of Australia, Canada, China, France, Italy, Japan, South Africa, UK and USA that funded the radars of the SuperDARN network (Dartmouth, 2022).

**Acknowledgments**
This work has partially been supported by Italian PNRA under contract PNRA18-00289-A "Space weather in Polar Ionosphere: the Role of Turbulence (SPIRiT)." G.L. acknowledges the PhD course in Astronomy, Astrophysics and Space Science of the University of Rome "Sapienza," University of Rome "Tor Vergata" and Istituto Nazionale di Geofisica e Vulcanologia, Italy.

## References

Buchert, S., Zangerl, F., Sust, M., André, M., Eriksson, A., Wahlund, J.-E., & Opgenoorth, H. (2015). Swarm observations of equatorial electron densities and topside GPS track losses. *Geophysical Research Letters*, *42*(7), 2088–2092. https://doi.org/10.1002/2015gl063121

Cherniak, I., & Zakharenkova, I. (2016). High-latitude ionospheric irregularities: Differences between ground-and space-based GPS measurements during the 2015 St. Patrick's Day storm. *Earth Planets and Space*, *68*(1), 1–13. https://doi.org/10.1186/s40623-016-0506-1

Chisham, G., Lester, M., Milan, S., Freeman, M., Bristow, W., Grocott, A., et al. (2007). A decade of the Super Dual Auroral Radar Network (superDARN): Scientific achievements, new techniques and future directions. *Surveys in Geophysics*, *28*(1), 33–109. https://doi.org/10.1007/s10712-007-9017-8

Clausen, L. B. N., & Moen, J. I. (2015). Electron density enhancements in the polar cap during periods of dayside reconnection. *Journal of Geophysical Research: Space Physics*, *120*(6), 4452–4464. https://doi.org/10.1002/2015JA021188

Coley, W., & Heelis, R. (1998). Structure and occurrence of polar ionization patches. *Journal of Geophysical Research*, *103*(A2), 2201–2208. https://doi.org/10.1029/97ja03345

Consolini, G., Tozzi, R., De Michelis, P., Coco, I., Giannattasio, F., Pezzopane, M., et al. (2021). High-latitude polar pattern of ionospheric electron density: Scaling features and IMF dependence. *Journal of Atmospheric and Solar-Terrestrial Physics*, *217*, 105531. https://doi.org/10.1016/j.jastp.2020.105531

Cowley, S. (1982). The causes of convection in the Earth's magnetosphere: A review of developments during the IMS. *Reviews of Geophysics*, *20*(3), 531–565. https://doi.org/10.1029/rg020i003p00531

Cowley, S., Morelli, J., & Lockwood, M. (1991). Dependence of convective flows and particle precipitation in the high-latitude dayside ionosphere on the X and Y components of the interplanetary magnetic field. *Journal of Geophysical Research*, *96*(A4), 5557–5564. https://doi.org/10.1029/90ja02063

Dartmouth. (2022). SuperDARN dynamic model. [Software]. Thayer School of Engineering at Dartmouth. Retrieved from https://sdnet.thayer.dartmouth.edu/models/dynamicmodel.php

De Michelis, P., Consolini, G., Pignalberi, A., Lovati, G., Pezzopane, M., Tozzi, R., et al. (2022). Ionospheric turbulence: A challenge for GPS loss of lock understanding. *Space Weather*, *20*(7), e03129. https://doi.org/10.1029/2022SW003129

De Michelis, P., Consolini, G., Tozzi, R., & Marcucci, M. F. (2017). Scaling features of high-latitude geomagnetic field fluctuations at swarm altitude: Impact of IMF orientation. *Journal of Geophysical Research (Space Physics)*, *122*(10), 10548–10562. https://doi.org/10.1002/2017JA024156

Dods, J., Chapman, S., & Gjerloev, J. (2017). Characterizing the ionospheric current pattern response to southward and northward IMF turnings with dynamical supermag correlation networks. *Journal of Geophysical Research: Space Physics*, *122*(2), 1883–1902. https://doi.org/10.1002/2016ja023686

ESA. (2022). Swarm data access. [Dataset]. European Space Agency. Retrieved from https://swarm-diss.eo.esa.int/

Fear, R. C. (2021). The northward IMF magnetosphere. *Magnetospheres in the solar system*, 293–309. https://doi.org/10.1002/9781119815624.ch19

Friis-Christensen, E., Lühr, H., Knudsen, D., & Haagmans, R. (2008). Swarm an Earth observation mission investigating geospace. *Advances in Space Research*, *41*(1), 210–216. https://doi.org/10.1016/j.asr.2006.10.008

Greenwald, R. A., Shepherd, S. G., Sotirelis, T. S., Ruohoniemi, J. M., & Barnes, R. J. (2002). Dawn and dusk sector comparisons of small-scale irregularities, convection, and particle precipitation in the high-latitude ionosphere. *Journal of Geophysical Research*, *107*(A9), SIA-1.

Haaland, S., Paschmann, G., Förster, M., Quinn, J., Torbert, R., McIlwain, C., et al. (2007). High-latitude plasma convection from cluster EDI measurements: Method and IMF-dependence. In *Annales geophysicae* (Vol. 25, pp. 239–253).

Jin, Y., & Oksavik, K. (2018). GPS scintillations and losses of signal lock at high latitudes during the 2015 St. Patrick's Day storm. *Journal of Geophysical Research: Space Physics*, *123*(9), 7943–7957. https://doi.org/10.1029/2018ja025933

Jin, Y., Spicher, A., Xiong, C., Clausen, L. B., Kervalishvili, G., Stolle, C., & Miloch, W. J. (2019). Ionospheric plasma irregularities characterized by the Swarm satellites: Statistics at high latitudes. *Journal of Geophysical Research: Space Physics*, *124*(2), 1262–1282. https://doi.org/10.1029/2018JA026063

Jin, Y., Xiong, C., Clausen, L., Spicher, A., Kotova, D., Brask, S., et al. (2020). Ionospheric plasma irregularities based on in situ measurements from the Swarm satellites. *Journal of Geophysical Research: Space Physics*, *125*(7), e2020JA028103. https://doi.org/10.1029/2020ja028103

Karpachev, A., Deminova, G., & Pulinets, S. (1995). Ionospheric changes in response to IMF variations. *Journal of Atmospheric and Terrestrial Physics*, *57*(12), 1415–1432. https://doi.org/10.1016/0021-9169(94)00141-a

Liu, Y., Fu, L., Wang, J., & Zhang, C. (2017). Study of GNSS loss of lock characteristics under ionosphere scintillation with GNSS data at Weipa (Australia) during solar maximum phase. *Sensors*, *17*(10), 2205. https://doi.org/10.3390/s17102205

Lockwood, M., Cowley, S., & Freeman, M. (1990). The excitation of plasma convection in the high-latitude ionosphere. *Journal of Geophysical Research*, *95*(A6), 7961–7972. https://doi.org/10.1029/ja095ia06p07961

Lockwood, M., McCrea, I., Milan, S. E., Moen, J., Cerisier, J., & Thorolfsson, A. (2000). Plasma structure within poleward-moving cusp/cleft auroral transients: EISCAT Svalbard radar observations and an explanation in terms of large local time extent of events. In *Annales geophysicae* (Vol. 18, pp. 1027–1042).

Moen, J., Hosokawa, K., Gulbrandsen, N., & Clausen, L. B. N. (2015). On the symmetry of ionospheric polar cap patch exits around magnetic midnight. *Journal of Geophysical Research: Space Physics*, *120*(9), 7785–7797. https://doi.org/10.1002/2014ja020914

Moen, J., Qiu, X., Carlson, H., Fujii, R., & McCrea, I. (2008). On the diurnal variability in F2-region plasma density above the EISCAT Svalbard radar. In *Annales geophysicae* (Vol. 26, pp. 2427–2433).

Murr, D., & Hughes, W. (2001). Reconfiguration timescales of ionospheric convection. *Geophysical Research Letters*, *28*(11), 2145–2148. https://doi.org/10.1029/2000gl012765

NASA. (2022). OMNIWeb data explorer. [Dataset]. OMNI, NASA. Retrieved from https://omniweb.gsfc.nasa.gov/form/dx1.html

Peng, Z., Wang, C., & Hu, Y. (2010). Role of IMF $B_x$ in the solar wind-magnetosphere-ionosphere coupling. *Journal of Geophysical Research*, *115*(A8), e2019GL086062. https://doi.org/10.1029/2010ja015454

Pezzopane, M., Pignalberi, A., Coco, I., Consolini, G., De Michelis, P., Giannattasio, F., et al. (2021). Occurrence of GPS loss of lock based on a swarm half-solar cycle dataset and its relation to the background ionosphere. *Remote Sensing*, *13*(11), 2209. https://doi.org/10.3390/rs13112209

Richmond, A. D. (1995). Ionospheric electrodynamics using magnetic apex coordinates. *Journal of Geomagnetism and Geoelectricity*, *47*(2), 191–212. https://doi.org/10.5636/jgg.47.191

Ruohoniemi, J., & Baker, K. (1998). Large-scale imaging of high-latitude convection with Super Dual Auroral Radar Network HF radar observations. *Journal of Geophysical Research*, *103*(A9), 20797–20811. https://doi.org/10.1029/98ja01288

Ruohoniemi, J., & Greenwald, R. (1996). Statistical patterns of high-latitude convection obtained from Goose Bay HF radar observations. *Journal of Geophysical Research*, *101*(A10), 21743–21763. https://doi.org/10.1029/96ja01584

Ruohoniemi, J., Greenwald, R., De la Beaujardiere, O., & Lester, M. (1993). The response of the high-latitude dayside ionosphere to an abrupt northward transition in the IMF. In *Annales geophysicae* (Vol. 11, pp. 544–555).

Spicher, A., Clausen, L. B. N., Miloch, W. J., Lofstad, V., Jin, Y., & Moen, J. I. (2017). Interhemispheric study of polar cap patch occurrence based on swarm in situ data. *Journal of Geophysical Research: Space Physics*, *122*(3), 3837–3851. https://doi.org/10.1002/2016JA023750

Tanaka, T. (2007). Magnetosphere-ionosphere convection as a compound system. *Space Science Reviews*, *133*(1–4), 1–72. https://doi.org/10.1007/s11214-007-9168-4

Teunissen, P. J., & Montenbruck, O. (2017). *Springer handbook of global navigation satellite systems* (Vol. 10). Springer.

Tsunoda, R. T. (1988). High-latitude F-region irregularities: A review and synthesis. *Reviews of Geophysics*, *26*(4), 719–760. https://doi.org/10.1029/RG026i004p00719

van den IJssel, J., Encarnação, J., Doornbos, E., & Visser, P. (2015). Precise science orbits for the Swarm satellite constellation. *Advances in Space Research*, *56*(6), 1042–1055. https://doi.org/10.1016/j.asr.2015.06.002

Xiong, C., Stolle, C., & Park, J. (2018). Climatology of GPS signal loss observed by Swarm satellites. *Annales Geophysicae*, *36*(2), 679–693. https://doi.org/10.5194/angeo-36-679-2018

Xiong, C., Yin, F., Luo, X., Jin, Y., & Wan, X. (2019). Plasma patches inside the polar cap and auroral oval: The impact on the spaceborne GPS receiver. *Journal of Space Weather and Space Climate*, *9*, A25. https://doi.org/10.1051/swsc/2019028

Yu, Y., & Ridley, A. J. (2009). Response of the magnetosphere-ionosphere system to a sudden southward turning of interplanetary magnetic field. *Journal of Geophysical Research*, *114*(A3), A03216. https://doi.org/10.1029/2008ja013292

Zhang, S., He, L., & Wu, L. (2020). Statistical study of loss of GPS signals caused by severe and great geomagnetic storms. *Journal of Geophysical Research: Space Physics*, *125*(9), e2019JA027749. https://doi.org/10.1029/2019ja027749